Comprehensive Finite-Difference Time-Dependent Beam Propagation Model of Counterpropagating Picosecond Pulses in a Semiconductor Optical Amplifier

Mohammad Razaghi, *Student Member, IEEE*, Vahid Ahmadi, *Member, IEEE*, and Michael J. Connelly, *Member, IEEE*

Abstract—In this paper, we present a numerical model to study counter pulse propagation in semiconductor optical amplifiers. An improved finite-difference beam propagation method for solving the modified nonlinear Schrödinger equation is applied for the first time in the counterpropagation regime. In our model, group velocity dispersion, two-photon absorption, ultrafast nonlinear refraction, and the change in the gain peak wavelength with carrier density are included, which have not been considered simultaneously in previous counterpropagation models. The model is applied to demonstrate how a subpicosecond and picosecond probe pulse shape and spectrum can be modified by a counterpropagating pump pulse. Based on the results obtained by this model, while subpicosecond probe pulses can be compressed by in this scheme, their time-bandwidth product are also improved significantly. Furthermore, the effects of several parameters are analyzed to obtain the proper probe spectral peak shift using counterpropagating probe pulses. The accuracy and computational efficiency of the new scheme are assessed through numerical examples and are shown to be superior to previously published approaches.

Index Terms—Counterpropagation, pulse shaping, semiconductor optical amplifier, ultrafast nonlinear effects.

I. INTRODUCTION

ULTRAHIGH-speed optical communication systems require all-optical signal processing schemes such as wavelength converters, all-optical modulators, demultiplexers, and 3R regenerators. These schemes are based on nonlinear effects with very fast dynamics in fiber or in semiconductor devices. Semiconductor optical amplifiers (SOAs) are a promising choice for their significant characteristics such as optical gain, low input power requirement, small size, capability of large-scale integration, and short response time. The

M. Razaghi and V. Ahmadi are with the Department of Electrical Engineering, Tarbiat Modares University, 14115-143 Tehran, Iran (e-mail: m.razaghi@uok.ac.ir; v_ahmadi@modares.ac.ir).

M. J. Connelly is with Optical Communications Research Group, Department of Electronic and Computer Engineering, University of Limerick, Limerick, Ireland (e-mail: michael.connelly@ul.ie; www.ece.ul.ie/research/ocrg/ocrg.htm).

Color versions of one or more of the figures in this paper are available online at http://ieeexplore.ieee.org.

Digital Object Identifier 10.1109/JLT.2008.2008823

theoretical investigation of ultrashort-pulse propagation in SOA is of fundamental importance for understanding of carrier dynamics and the nonlinear effects that determine pulse shaping and four-wave mixing (FWM) between short pulses [1].

Two main categories of SOA dynamic models can be distinguished: time- and frequency-domain models. Copropagation time-domain models can normally be solved easily using a single marching algorithm because the waves propagate only in one direction [2]. Counterpropagation time-domain models are significantly more complicated and consequently require more advanced numerical techniques to solve. Such techniques require significantly more computation time [3]. Furthermore, two boundary conditions at both ends of the SOA must be satisfied.

Counterpropagation modeling of the SOA plays an essential role in modeling systems such as terahertz optical asymmetric demultiplexers [4], optical logic gates [5], [6], mode-locked lasers [7], and wavelength converters [8], [9]. Furthermore, using the SOA in counterpropagation configuration shows a faster gain recovery, that is necessary in all-optical high bit-rate applications [10], and also improves the output extinction ratio in all-optical switching applications [11]. Moreover, this type of configuration brings about an increase in the capacity of the optical link in counterpropagation FWM applications [12].

The relevant effects that have to be considered in picosecond pulse amplification in an SOA model are interband (slow) gain dynamics [13], interband refractive index dynamics [14], carrier heating (CH) and spectral hole burning (SHB) [15], [16], two-photon absorption (TPA), ultrafast nonlinear refraction (UNR) [17]–[19], gain dispersion [20], gain peak shift with carrier density [21], [22], and group velocity dispersion (GVD) [23]. One should account for these effects to have a comprehensive reliable model in order to determine and understand the SOA high-speed dynamics, especially in terms of response times and optimizing SOA parameters for all-optical signal processing applications.

Different models have been used for the analysis of counterpropagation in SOAs. The multisection method [3], [24] and transfer-matrix method [21] model SOAs are using frequency domain techniques. These methods are not accurate in the picosecond regime. This is because they do not include TPA and UNR. Several time-domain models are based on the density matrix method [12], [25]. In these models, GVD and carrier dependency of the gain peak wavelength are neglected, which leads to large error in predicating the FWM pulse resulting from mixing

between pulses with large detuning. Recently in [26], a new analysis method of counterpropagating optical pulses in SOA has been proposed. This time-domain model does not consider important nonlinear effects including SHB, CH, TPA, and gain dispersion, so it can not be reliable for modeling picosecond and subpicosecond counterpropagating pulses in SOAs.

The beam propagation method (BPM) is the most widely used method for the study of light propagation in optical waveguides devices [27]–[29]. It uses a spectral propagation algorithm to propagate an arbitrary incident beam through a medium of slowly varying refractive index. This method has already been used for the simulation of optical pulse propagation in SOAs [23].

In this paper, we use for the first time an improved finite-difference BPM (IFDBPM), to model the temporal and spectral properties of copropagating and counterpropagating picosecond optical pulses with different wavelengths, which are injected into an SOA. This time evolution method is basically simple, efficient, and powerful especially when applied to model counter pulse propagation.

The analysis is based on a modified nonlinear Schrödinger equation (MNLSE) considering GVD, interband gain dynamics, interband refractive index dynamics, TPA, UNR, CH, SHB, their dispersions, and gain dispersion in an SOA. We also consider the gain peak shift with carrier density. Based on this model, we study the effects of counterpropagating pump pulse on probe pulse shape and spectrum in subpicosecond regime, which to our knowledge has not been reported before.

This paper is organized as follows. In the next section, we introduce our modeling scheme based on an IFDBPM. In Section III, we show simulation results for different scenarios, showing the effects of SOA dynamic gain on picosecond single- and multiple-pulse amplification in both copropagating and counterpropagating regimes. We also model the FWM pulse resulting from copropagating pump and probe pulses. The effects of counterpropagating pump pulse on subpicosecond probe pulse shape and spectrum are also investigated. Conclusions are presented in Section IV.

II. ANALYTICAL MODEL

The forward and backward propagating optical fields with complex amplitude $A^{\pm}(z,t)$ for counterpropagation scheme are determined from the solution to the MNLSE given by [18]

$$
\begin{aligned}
&\left[\pm\frac{\partial}{\partial z} + \frac{1}{\nu_g}\frac{\partial}{\partial t}\right] A^{\pm}(z,t) \\
&= \left\{ \frac{i}{2}\beta_2\frac{\partial^2}{\partial t^2} - \left(\frac{\gamma_{2p}}{2}+ib_2\right)I(z,t) - \frac{\gamma}{2} + \frac{1}{2}g_N(t) \right. \\
&\quad \times\left[\frac{1}{f_T(t)}+i\alpha_N\right] + \frac{1}{2}\Delta g_T(t)[1+i\alpha_T] - i\left.\frac{1}{2}\frac{\partial g(t,\omega)}{\partial\omega}\right|_{\omega_0} \\
&\quad \left. \times\frac{\partial}{\partial t} - \frac{1}{4}\left.\frac{\partial^2 g(t,\omega)}{\partial\omega^2}\right|_{\omega_0}\frac{\partial^2}{\partial t^2} \right\} A^{\pm}(z,t)
\end{aligned} \tag{1}
$$

where

$$
g_N(t) = g_0 \exp\left(-\frac{1}{E_{\text{sat}}}\int_{-\infty}^{+\infty} U(s)e^{-s/\tau_s}I(z,t)ds\right) \tag{2}
$$

$$
\begin{aligned}
\Delta g_T(t) = &-h_1\int_{-\infty}^{+\infty} U(s)e^{-s/\tau_{\text{CH}}}(1-e^{-s/\tau_{\text{SHB}}})I(z,t)ds \\
&-h_2\int_{-\infty}^{+\infty} U(s)e^{-s/\tau_{\text{CH}}}(1-e^{-s/\tau_{\text{SHB}}})I'(z,t)ds
\end{aligned} \tag{3}
$$

$$
f_T(t) = 1 + \frac{1}{\tau_{\text{SHB}}P_{\text{SHB}}}\int_{-\infty}^{+\infty} U(s)e^{-s/\tau_{\text{SHB}}}I(z,t)ds \tag{4}
$$

$$
\left.\frac{\partial g(t,\omega)}{\partial\omega}\right|_{\omega_0} = A_1 + B_1[g_0 - g(t,\omega_0)] \tag{5}
$$

$$
\left.\frac{\partial^2 g(t,\omega)}{\partial\omega^2}\right|_{\omega_0} = A_2 + B_2[g_0 - g(t,\omega_0)] \tag{6}
$$

$$
g(t,\omega_0) = \frac{g_N(t,\omega_0)}{f_T(t)} + \Delta g_T(t,\omega_0). \tag{7}
$$

The slowly varying envelope approximation is used in (1), where the temporal variation change of the complex envelope function is very slow compared with the cycle of an optical field. In (1), $A^{+}(z,t)$, $A^{-}(z,t)$ are the forward and backward time-domain complex envelope functions of an optical pulse, $I(z,t)$ is the photon density given by $I(z,t) = |A^{+}(z,t)|^2 + |A^{-}(z,t)|^2$ and $I'(z,t) = |A^{+}(z,t)|^4 + |A^{-}(z,t)|^4$, β_2 is the GVD coefficient, and v_g is the group velocity at transparency. γ is the linear loss, $b_2(=\omega_0 n_2/cA_r)$ is the instantaneous self-phase modulation term due to the UNR, n_2 is the Kerr effect coefficient, ω_0 is the center angular frequency of the pulse, c is the velocity of light in vacuum, $A_r(=wd/\Gamma)$ is the effective area (d and w are the thickness and width of the active region, respectively, and Γ is the confinement factor). $g_N(t)$ is the saturated gain due to carrier depletion [16], g_0 is the linear gain, E_{sat} is the saturation energy, τ_s is the carrier lifetime, $f_T(t)$ is the SHB function [17], P_{SHB} is the SHB saturation power, τ_{SHB} is the SHB relaxation time, and α_N and α_T are the linewidth enhancement factors associated with the gain change due to carrier depletion and CH. $\Delta g_T(t)$ is the resulting gain change due to the CH and TPA, $U(s)$ is the unit step function, τ_{CH} is the CH relaxation time. γ_{2p}, h_1, and h_2 are phenomenological constants including the strength of TPA, the contribution of stimulated emission and free carrier absorption to CH included gain reduction and the contribution of TPA, respectively. Finally, A_1 and A_2 are the slope and the curvature of the linear gain at ω_0, respectively, while B_1 and B_2 are constants describing changes in these quantities with saturation [18]. Fig. 1 shows the gain spectra given by second-order Taylor expansion about the pulse center angular frequency (ω_0) for AlGaAs/GaAs bulk SOA. A_1, A_2, B_1, and B_2 are used from [30]. The dependency of gain peak on carrier density can be obtained, which agrees well with experimental results [30].

The most straightforward approach to solve coupled nonlinear partial differential equations such as (1) is to approximate each derivative in time and space using a finite difference. Zhang *et al.* [31] and Adachihara *et al.* [32] have used such a method to study laser dynamics in the nanosecond range. For picosecond pulse propagation problems, however, such a double differentiation approach is not appropriate for several reasons. Besides
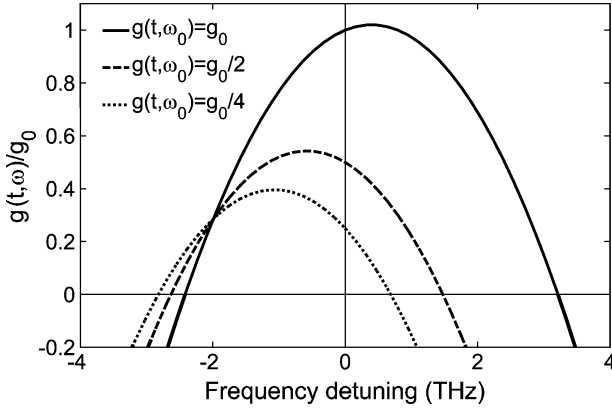
Fig. 1. The gain spectra given by the second-order Taylor expansion about the pulse center frequency, with derivatives of $g(t, \omega)$ by (5) and (6).

the computational effort required for the fine division in space and time, it can be an unstable method [33]. Recently, Chi *et al.* [26] has used the first-order forward finite difference (FDM) for solving coupled basic pulse propagation equations in the counterpropagating regime. In this method, however, if some nonlinear terms of the MNLSE such as gain dispersion and GVD are included, the finite-difference approach can not be used to solve the resulting modified equation. Furthermore, if the frequency dependency of the propagated pulse is included in the basic pulse propagation equations, they can not be solved using the FDM. Consequently, Chi's model neglects frequency dependency and is therefore unable to investigate FWM phenomenon.

Different methods have been proposed for solving the nonlinear Schrödinger equation in the copropagating regime. These methods include the split-step Fourier transform method (SSFM) [34] and FDBPM [23]. The presence of first- and second-order gain dispersion in the MNLSE makes it impossible to separate the linear and nonlinear terms in (1). As the implementation of SSFM requires such a separation, it is not possible to solve (1) using this method.

For solving nonlinear propagation equations such as the MNLSE for counterpropagating pulses, we used a trapezoidal integration and central difference technique. Using this method, a set of MNLSEs in the counterpropagation regime can be solved with high precision in just a few seconds on a desktop computer.

To solve (1), we introduce two space-time variables u^+ and u^- defined as

$$u^+ = (T + z)/2$$
$$u^- = (T - z)/2. \tag{8a}$$

The inverse relations are

$$z = u^+ - u^-$$
$$T = u^+ + u^- \tag{8b}$$

where $T = v_g t (\mathrm{m})$. If the time derivative on the right-hand side of (1) is replaced by central difference approximation and (8a)

is applied, the equivalent equation in coordinates (u^+, u^-) is obtained

$$
\begin{aligned}
\frac{\partial}{\partial u^\pm} & A^\pm(u^+, u^-) \\
= & \left\{ i \frac{v_g^2}{2\Delta^2} \beta_2 - i \frac{v_g}{4\Delta} \left.\frac{\partial g}{\partial \omega}\right|_{\omega_0} - \frac{v_g^2}{4\Delta^2} \left.\frac{\partial^2 g}{\partial \omega^2}\right|_{\omega_0} \right\} \\
& \times A^\pm(u^+ - \Delta/2, u^- - \Delta/2) \\
& - \left\{ i \frac{v_g^2}{\Delta^2} \beta_2 + \frac{\gamma}{2} + v_g \left(\frac{\gamma_{2p}}{2} + ib_2 \right) I(u^+, u^-) \right. \\
& \quad - \frac{1}{2} g_N \left[\frac{1}{f_T} + i\alpha_N \right] - \frac{1}{2} \Delta g_T [1 + i\alpha_T] \\
& \quad \left. - \frac{v_g^2}{2\Delta^2} \left.\frac{\partial^2 g}{\partial \omega^2}\right|_{\omega_0} \right\} A^\pm(u^+, u^-) \\
& + \left\{ i \frac{v_g^2}{2\Delta^2} \beta_2 + i \frac{v_g}{4\Delta} \left.\frac{\partial g}{\partial \omega}\right|_{\omega_0} - \frac{v_g^2}{4\Delta^2} \left.\frac{\partial^2 g}{\partial \omega^2}\right|_{\omega_0} \right\} \\
& \times A^\pm(u^+ + \Delta/2, u^- + \Delta/2) \tag{9}
\end{aligned}
$$

where Δ is the step size defined as L/M, where L is the SOA length and M is number of section. Based on this new definition, the forward- and backward-propagating fields at each step are related to adjacent steps.

The solution of [(2)–(7)] and (9), requires the use of numerical techniques. High-order methods such as the Runge–Kutta approach [33], [35] and first-order FDM [26] have been proposed to solve such equations. As the right-hand side of (9) is not constant, the Runge–Kutta method is not a proper choice. Furthermore, convergence does not occur if the FDM is used to solve (9).

We use trapezoidal integration for solving (9). If we integrate (9) over u^+ and u^-, respectively, with a small propagation step Δ, two tridiagonal simultaneous matrices are obtained.

$$
\begin{aligned}
& - a^+(u^+ + \Delta, u^-) \times A^+(u^+ + \Delta/2, u^- - \Delta/2) \\
& \quad + \left[1 - b^+(u^+ + \Delta, u^-) \right] \times A^+(u^+ + \Delta, u^-) \\
& \quad - c^+(u^+ + \Delta, u^-) \times A^+(u^+ + 3\Delta/2, u^- + \Delta/2) \\
& = -a^+(u^+, u^-) \times A^+(u^+ - \Delta/2, u^- - \Delta/2) \\
& \quad + \left[1 - b^+(u^+, u^-) \right] \times A^+(u^+, u^-) \\
& \quad - c^+(u^+, u^-) \times A^+(u^+ + \Delta/2, u^- + \Delta/2) \tag{10} \\
& - a^-(u^+, u^- + \Delta) \times A^-(u^+ - \Delta/2, u^- + \Delta/2) \\
& \quad + \left[1 - b^-(u^+, u^- + \Delta) \right] \times A^-(u^+, u^- + \Delta) \\
& \quad - c^-(u^+, u^- + \Delta) \times A^-(u^+ + \Delta/2, u^- + 3\Delta/2) \\
& = -a^-(u^+, u^-) \times A^-(u^+ - \Delta/2, u^- - \Delta/2) \\
& \quad + \left[1 - b^-(u^+, u^-) \right] \times A^-(u^+, u^-) \\
& \quad - c^-(u^+, u^-) \times A^-(u^+ + \Delta/2, u^- + \Delta/2). \tag{11}
\end{aligned}
$$

The relationship between the new coordinates (u^+, u^-) and original coordinates (z, T) are shown in Fig. 2. It should be noted based on (8) that the step size in both (u^+, u^-) and (z, T) coordinates is Δ. For simplicity, two integers (m, N) are used
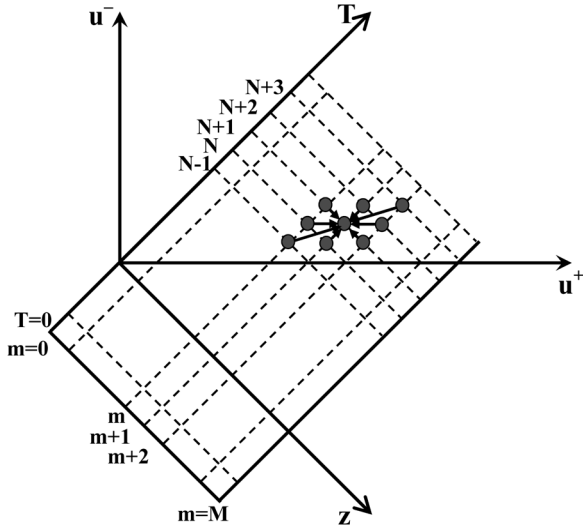
Fig. 2. Integration domain in the new coordinates u^+ and u^-. In the numerical algorithm the value of a quantity of interest at the $(m+1, N+1)$ spatial-time step depends on eight adjacent values as shown.

instead of (z, T) in the following equations so that $A(m, N)$ signifies $A(z = m\Delta, T = N\Delta)$.

To find the state of the system at each point, the state of eight adjacent points must be known as shown in Fig. 2.

Based on this new description (10) and (11) become

$$- a^+(m+1, N+1) \times A^+(m+1, N)$$
$$+ \left[1 - b^+(m+1, N+1)\right] \times A^+(m+1, N+1)$$
$$- c^+(m+1, N+1) \times A^+(m+1, N+2)$$
$$= -a^+(m, N) \times A^+(m, N-1)$$
$$+ \left[1 - b^+(m, N)\right] \times A^+(m, N)$$
$$- c^+(m, N) \times A^+(m, N+1) \qquad (12)$$

$$- a^-(m+1, N+1) \times A^-(m+1, N)$$
$$+ \left[1 - b^-(m+1, N+1)\right] \times A^-(m+1, N+1)$$
$$- c^-(m+1, N+1) \times A^-(m+1, N+2)$$
$$= -a^-(m+2, N+2) \times A^-(m+2, N+1)$$
$$+ \left[1 - b^-(m+2, N+2)\right] \times A^-(m+2, N+2)$$
$$- c^-(m+2, N+2) \times A^-(m+2, N+3) \qquad (13)$$

where

$$a^\pm(m, N) = \frac{\Delta}{2} \left[\frac{i\nu_g^2 \beta_2}{2\Delta^2} + \frac{i\nu_g}{4\Delta} \left. \frac{\partial g(N, \omega)}{\partial \omega} \right|_{\omega_0} \right.$$
$$\left. - \frac{\nu_g^2}{4\Delta^2} \left. \frac{\partial^2 g(N, \omega)}{\partial \omega^2} \right|_{\omega_0} \right] \qquad (14)$$

$$b^\pm(m, N) = - \frac{\Delta}{2} \left[\frac{i\nu_g^2 \beta_2}{\Delta^2} + \frac{\gamma}{2} + \nu_g \left(\frac{\gamma_{2p}}{2} + ib_2 \right) I(m, N) \right.$$
$$- \frac{\nu_g^2}{2\Delta^2} \left. \frac{\partial^2 g(N, \omega)}{\partial \omega^2} \right|_{\omega_0}$$
$$+ \frac{1}{2} \Delta g_T(N, \omega_0)[1 + i\alpha_T]$$
$$\left. - \frac{1}{2} g_N(N, \omega_0) \left[\frac{1}{f_T(N)} + i\alpha_N \right] \right] \qquad (15)$$

$$c^\pm(m, N) = \frac{\Delta}{2} \left[\frac{i\nu_g^2 \beta_2}{2\Delta^2} - \frac{i\nu_g}{4\Delta} \left. \frac{\partial g(N, \omega)}{\partial \omega} \right|_{\omega_0} \right.$$
$$\left. - \frac{\nu_g^2}{4\Delta^2} \left. \frac{\partial^2 g(N, \omega)}{\partial \omega^2} \right|_{\omega_0} \right]. \qquad (16)$$

It is not possible to directly calculate (12) and (13) because it is necessary to calculate the left-side terms $a^\pm(m+1, N+1)$, $b^\pm(m+1, N+1)$, and $c^\pm(m+1, N+1)$ of (12), (13) from the unknown $A^\pm(m+1, N)$, $A^\pm(m+1, N+1)$, and $A^\pm(m+1, N+2)$. We initially define $a^+(m+1, N+1) = a^+(m, N)$, $b^+(m+1, N+1) = b^+(m, N)$, and $c^+(m+1, N+1) = c^+(m, N)$ for the forward-propagating field and $a^-(m+1, N+1) = a^-(m+2, N+2)$, $b^-(m+1, N+1) = b^-(m+2, N+2)$, and $c^-(m+1, N+1) = c^-(m+2, N+2)$ for the backward-propagating field. With this estimation and using iteration procedure, the accurate results are obtained. A flowchart of the algorithm is shown in Fig. 3.

In this paper, we compare several simulations using different step sizes. It is found that good convergence with $M = 128$ can be achieved if the input pulsewidth is more than 10 ps but as the pulsewidth decreases to subpicosecond, *M* must be increased (e.g for 500 fs input pulsewidth, $M = 384$).

III. RESULTS AND DISCUSSION

To verify the precision of our method, the IFDBPM procedure was applied to some well-known SOA configurations.

A. Copropagation Simulation

The first case is the SOA model given by [13]. This analytical model is valid for pulses with pulsewidths >10 ps. In the model, the SPM phenomenon is the only nonlinear effect included in the propagation equation. To verify our model via comparison to the basic model, we set $\tau_s = \text{infinite}$, $\Delta g_T = 0$, $f_T = 0$, $\beta_2 = 0$, $\gamma_{2p} = 0$, $\gamma = 0$, $\partial g / \partial \omega = 0$, and $\partial^2 g / \partial^2 \omega = 0$. Other parameters are: $\alpha_N = 5$, $n_g = 4$ and $E_{\text{in}}/E_{\text{sat}} = 0.1$, where E_{in} is the energy of the unchirped Gaussian input pulse, with pulsewidth (full-width at half-maximum) $T_{\text{FWHM}} = 20$ ps. $g_0 L = 6.9$, which correspond to an unsaturated single pass gain (G_0) of 30 dB. The standard deviation between our simulation using $M = 128$ and Agrawal's analytical solution [13] is approximately 4%. Our simulation was also compared to Chi's model [26] with $M = 128$. As Fig. 4 shows, with $M = 128$ Chi's model is significantly different from Agrawal's solution. Chi's model requires $M = 1024$ to achieve an accuracy within 15% of Agrawal's model, which leads to very large computation time and memory compared with our model. Notice that the leading-edge sharpening of these amplified pulses originates from the gain saturation effect, which results in an apparently faster pulse peak transmission.

To show the applicability of our model in the subpicosecond regime, the model is compared with experimental results. The input pulse $(T_{\text{FWHM}} = 420 \text{ fs})$ used in the simulations is a synthesized pulse having the same temporal and spectral shape (spectral width = 1.26 THz) as the experimental input pulse in [18]. Fig. 5 shows the simulated output pulse temporal profile and spectrum from the SOA, which are in very good agreement with the experimental results in [18]. In our simulation we used
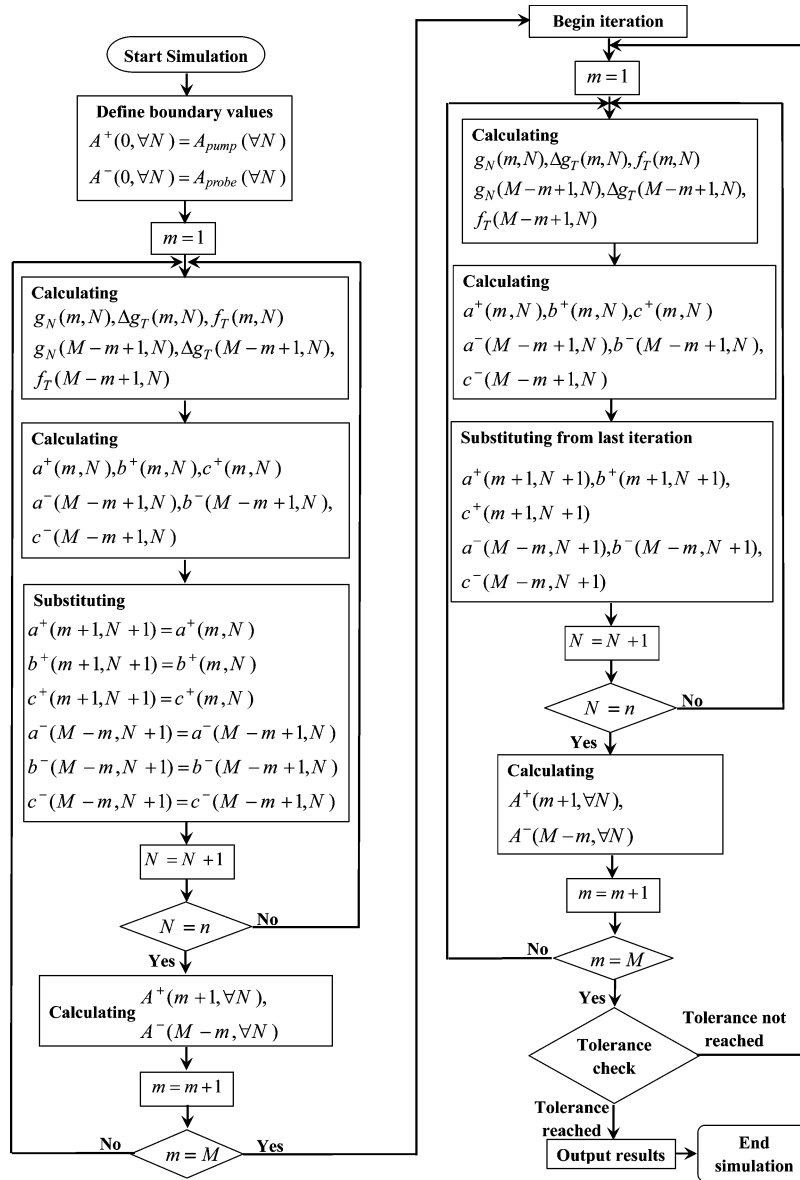
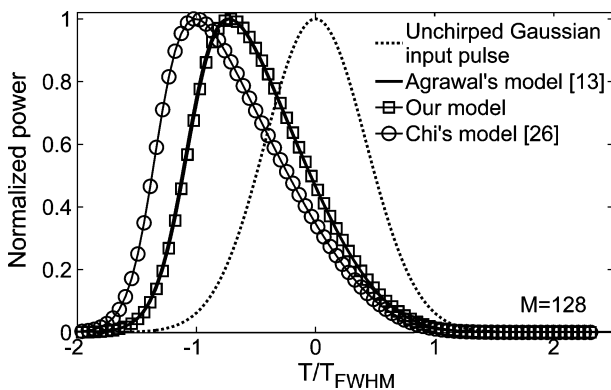Fig. 3. Counterpropagation IFDBPM algorithm, n is the final time iteration step.

Fig. 4. Normalized output pulse shapes for three different methods of calculations.

$M = 384$. These results are completely different from those predicted by Agrawal's model as shown in Fig. 5, because self-phase modulation is the only nonlinear process that is included in that model.

Next, we compare our model with Das's model [23] in which FWM between two copropagating pulses in an SOA was investigated. The input pulse complex amplitude can be written as

$$A(t) = A_p(t) + A_q(t)\exp(-i\Delta\omega t) \qquad (17)$$

where $A_p(t)$ and $A_q(t)$ are the complex envelope functions of the input pump and probe pulses, and $\Delta\omega$ is the pump–probe detuning expressed as $\Delta\omega = 2\pi(f_{\text{pump}} - f_{\text{probe}})$. The model parameters are listed in Table I [30].

Fig. 6 shows the simulation results when two input optical pulses with a pulsewidth of 10 ps propagate in an SOA. The input pulse shapes are sech^2 and are Fourier transform limited. The input energy of the pump and probe pulse are 2 pJ and 0.2 pJ, respectively. The pump–probe detuning is 1 THz. Fig. 6(a) shows the total output pulse power. A beat is observed in the
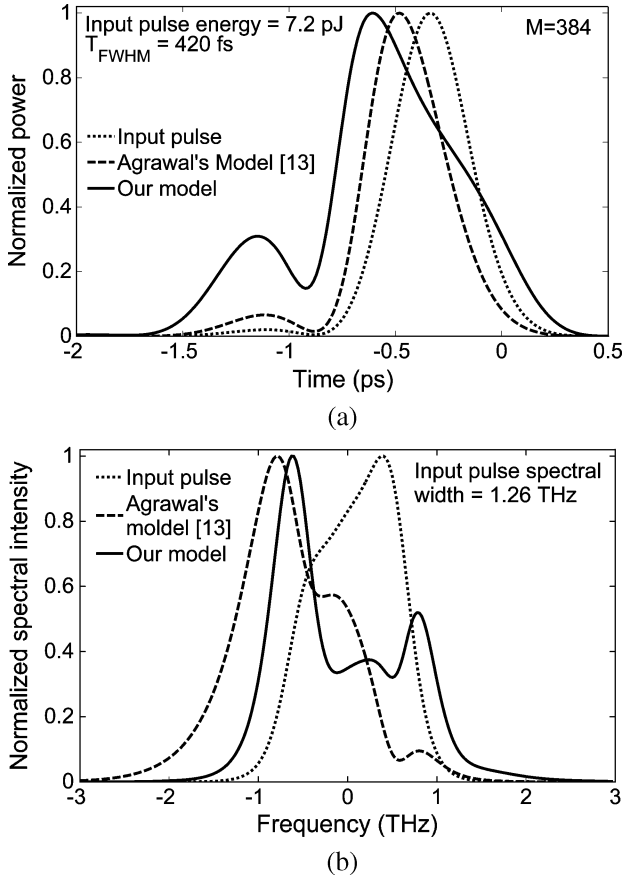
Fig. 5. Calculated output pulse (a) shape and (b) spectrum for two different methods of calculations.

TABLE I
LIST OF PARAMETERS USED IN SIMULATION [30]

Symbol	Quantity	Value
L	SOA length	500 μm
A_r	Effective area	5 μm²
f_0	Center frequency of the pulse	349 THz
g_0	Linear gain	92 cm⁻¹
β_2	Group velocity dispersion	0.05 ps²cm⁻¹
E_{sat}	Saturation energy	80 pJ
α_N	Linewidth enhancement factor due to the carrier depletion	3.1
α_T	Linewidth enhancement factor due to the carrier heating	2.0
h_1	The contribution of stimulated emission and free carrier absorption to the carrier heating gain reduction	0.13 cm⁻¹pJ⁻¹
h_2	The contribution of two photon absorption	126 fs cm⁻¹pJ⁻²
τ_s	Carrier lifetime	200 ps
τ_{CH}	Carrier heating relaxation time	700 fs
τ_{SHB}	Spectral –hole burning relaxation time	60 fs
P_{SHB}	Spectral –hole burning relaxation power	28.3 W
γ	Linear loss	11.5 cm⁻¹
n_2	Instantaneous nonlinear Kerr effect	-0.70 cm²TW⁻¹
γ_{2p}	Two photon absorption coefficient	1.1 cm⁻¹W⁻¹
A_1		0.15 fs μm⁻¹
A_2	Parameters describing second order Taylor	-80 fs
B_1	expansion of the dynamically gain spectrum	-60 fs² μm⁻¹
B_2		0 fs²

pulse shape, whose beat frequency depends on the detuning. Fig 6(b) shows the frequency spectrum of the total output pulse. In the output spectrum, both the pump and the probe peak wavelengths are redshifted. Moreover, some oscillatory structures are observed on the high frequency side of the amplified pump and probe pulses and FWM signal. These are attributed to the self-phase modulation effect by the change of the refractive index due to the gain saturation [13]. The output pump, probe, and FWM pulses are obtained by filtering the output pulse spectrum and taking the inverse Fourier transform. Fig. 7 shows the output waveforms of the pump, probe pulses, and the FWM signal pulse. Our results are in excellent agreement with Das's model results in [23].

B. Counterpropagation Simulations

The next case is to demonstrate the power of our method in counterpropagation configurations such as the system shown in [36]. In this work, the effect of the dynamic gain saturation on counterpropagating pulses in an SOA is investigated. This effect is studied by injecting two 14 ps (FWHM) counterpropagating, unchirped Gaussian pulses into the SOA. The pump pulse is delayed by 2 ps relative to the probe pulse, measured by the arrival time of the pulse peaks at their respective inputs. The energy of the input pulses is equal to $E_{sat}/20$. Other SOA parameters are $\alpha_N = 5$, $L = 500$ μm and $\tau_s = 0.1$ ns. Fig. 8 shows the probe pulse shapes and spectrums for unsaturated gains (G_0) of 20

dB and 30 dB. In our simulation $M = 128$. While, the results are in good agreement with those presented in [36], our algorithm is more computationally efficient. Self-phase modulation is the only nonlinear effect considered in [36]; however, the effects of other nonlinearities shown in (1) can not be neglected if the input pulsewidth is decreased to few picoseconds. To show the importance of these effects, we introduce the compression factor percentage (CFP) as

$$\text{CFP} = \frac{\text{Output probe pulsewidth} - \text{Input probe pulsewidth}}{\text{Input probe pulsewidth}} \times 100. \quad (18)$$

The effects of nonlinearities such as TPA, CH, SHB, Kerr effects, and gain dispersion on the probe pulsewidth are shown in Fig. 9. The parameters are used from Table I. As the input probe pulsewidth become shorter the output probe pulsewidth becomes wider and the effects of nonlinearities become more noticeable.

Nonlinear effects become more important in the subpicosecond regime. The effect of nonlinearities on the output pump and probe pulse shape is shown in Fig. 10, where the pump and probe pulsewidths are 500 fs and their energies are 0.1 pJ. The input pulse shapes are sech² and are Fourier transform limited. The pump pulse is injected 2 ps before the probe pulse. The unsaturated gain is 20 dB. As shown in Fig. 10, both output pulses are broadened due to the nonlinearities. The effect of nonlinearities on the output probe chirp is shown in Fig. 11. SHB and CH phenomena, unlike SPM, impose a
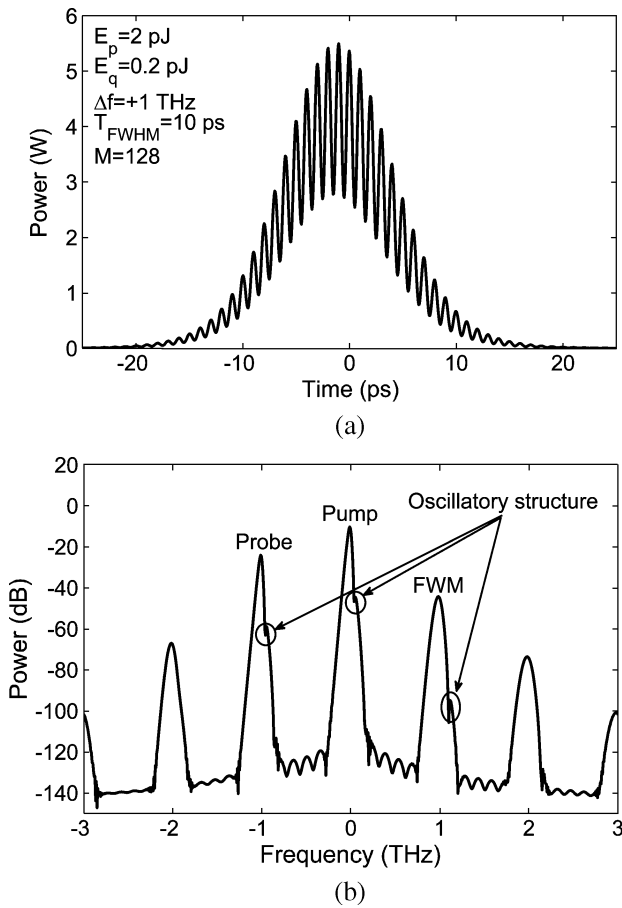
(a)

(b)

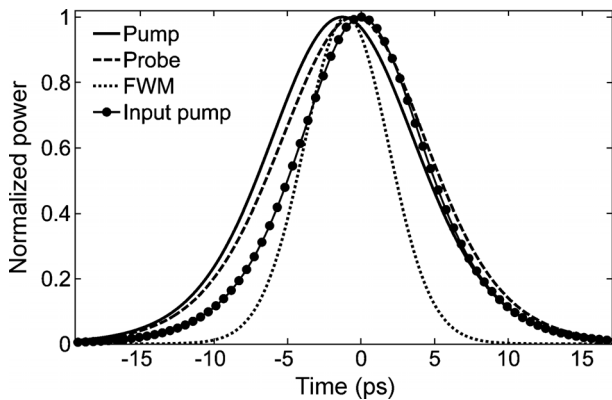Fig. 6. Calculated output pulse (a) shape and (b) spectrum.

Fig. 7. Output pump, probe pulse, and FWM signal shapes obtained from the output spectrum of Fig. 6. Output energies are 54 pJ, 2.18 pJ, and 0.04 pJ, respectively.
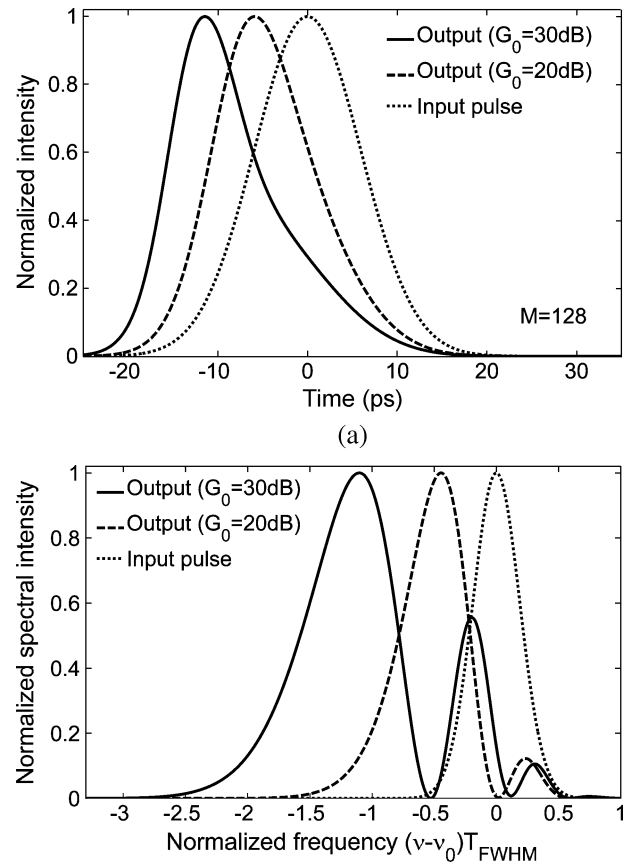

(a)

Fig. 8. Output pulses for probe pulses in the presence of a counterpropagation pulse: (a) shape, (b) spectrum. The only nonlinear effect included is SPM.
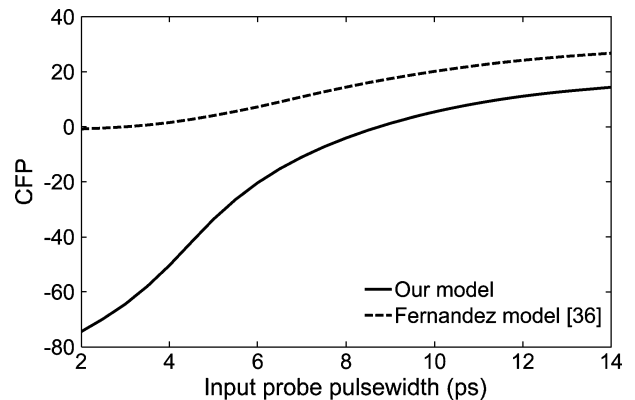

Fig. 9. CFP in presence of all nonlinearities (our model) and including SPM only (Fernandez's model [36]).

positive chirp on the propagated pulse as shown in Fig. 11. In subpicosecond regime, SHB in particular significantly affects the amplified pulse shapes.

Fig. 12 shows the spatio-temporal behavior of the dynamic gain, when all nonlinear effects are included and when only SPM is taken into account. In Fig. 12(a), all the nonlinear effects are considered. For subpicosecond pulses, the collision between pump and probe pulses leads to a dip shape reduction in the spatio-temporal gain profile. In addition the recovery time

of dynamic gain is primarily due to the SHB, time constant. It shows a considerable dip on output amplified pump and probe pulse at both ends of SOA waveguide. In contrast, in Fig. 12(b), where only SPM is considered, the recovery time is due to the relatively much longer carrier lifetime.

The effect of GVD on short-pulse propagation is shown in Fig. 13. To see the effect of GVD, the probe pulse energy should be low enough such that all other nonlinear effects are negligible. Therefore, input pulse energies are set to 1 fJ. The pump and probe pulses are injected at the same time. The input pulsewidths are 500 fs. For subpicosecond pulse propagation,
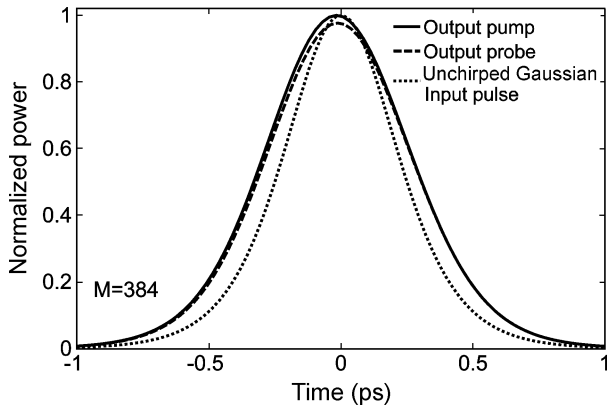
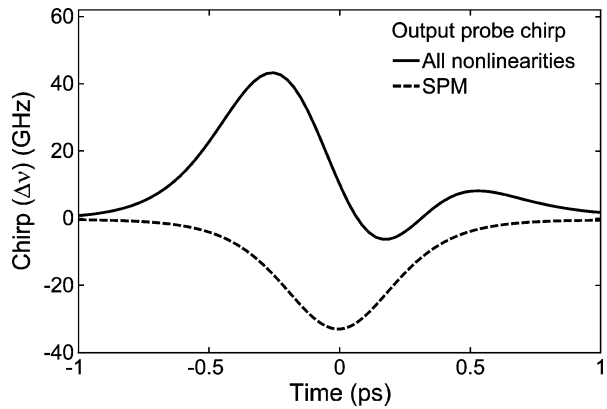Fig. 10. Output pump and probe pulse shapes. The input pulsewidths are 500 fs.

(a)

Fig. 11. Output probe chirp in presence of all nonlinearities and including SPM only.
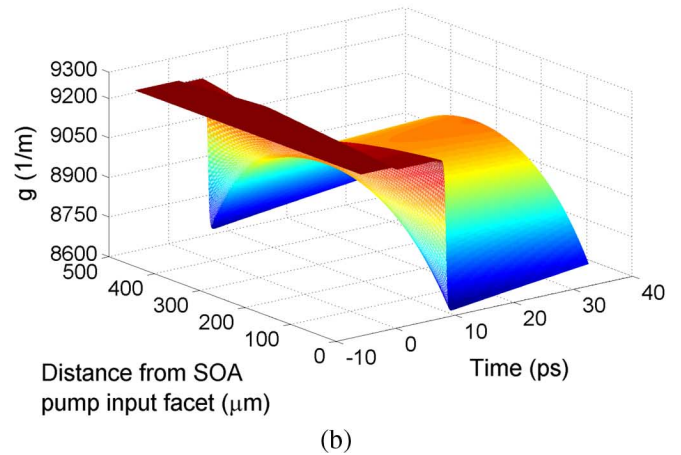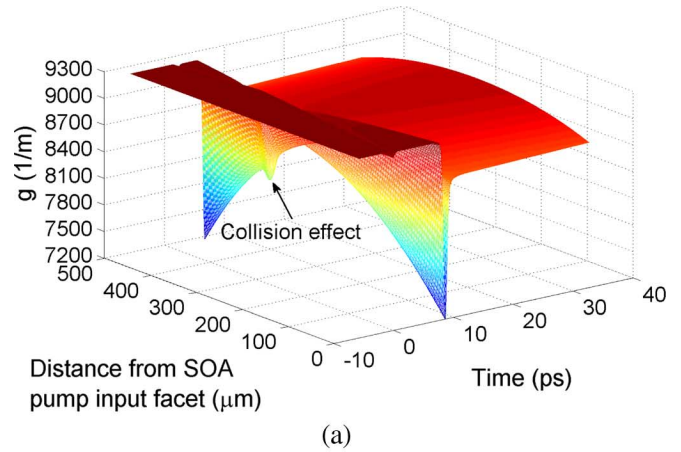

(b)

Fig. 12. Spatio-temporal dynamic gain in presence of (a) all nonlinearities and (b) SPM only.

GVD plays an important role in how copropagating and counterpropagating pulses interact. Fig. 13(a) shows the probe peak shift as a function of SOA length and detuning. The pulse peak shift is defined as the variation of the output pulse peak position from its input peak position in time domain. For typical SOA lengths this peak shift is of the order of 10 s of fs. Fig. 13(b) shows the pump peak shift as a function of SOA length and detuning in the case where the pump power is high enough to induce nonlinear effects in addition to intrinsic GVD. The peak shifts are typically in the range of 100–200 fs, so a comparison between Fig. 13(a) and (b) shows the GVD effect cannot be neglected especially for short pulses and for wide detuning.

The relative time delay between the injected pulses into an SOA can also significantly affect the amplified pulses in both the copropagation and counterpropagation schemes. Picosecond optical pulse compression of a probe pulse utilizing a copropagating pump pulse in an SOA was modeled in [37], where the GVD phenomena and effects of carrier depletion due to probe pulse are neglected. These approximations are inadequate in the subpicosecond regime where the GVD effect becomes important (Fig. 13) and when the pump and probe power become comparable (Fig. 8). In this paper, the change in the amplified probe pulse properties with different time delays between picosecond probe and the pump pulses in the counterpropagation scheme is

investigated. The parameters used for this simulation are listed in Table I. The input probe pulse is an unchirped Gaussian pulse with 14 ps pulsewidth. The powers of the probe and pump pulse are 0.05 pJ and 8 pJ, respectively, and the unsaturated gain is 30 dB. A comparison between copropagation and counterpropagation when both input pulses are injected simultaneously into an SOA is shown in Fig. 14. This figure shows that better pulse compression can be achieved in the counterpropagation scheme for input pump pulsewidths larger than 11 ps. Beside this in the counterpropagation scheme, the output probe is always amplified more in comparison to the copropagation scheme. The amplification factor is defined as the ratio of output probe pulse energy to input probe pulse energy. To compare the pulse compression and amplification characteristics of the copropagation and counterpropagation schemes care must be taken on parameters, such as the pump peak power and pulsewidth. The location where gain saturation becomes significant in an SOA waveguide is related to the pump pulse parameters. In the short pump pulse regime, for a given input pump pulse energy, this location is close to pump injection facet, and penetrates further into the SOA as the pump pulsewidth increases. Therefore, for short pulses, when both the pump and probe pulses are injected from the same facet, the overlap between the saturated media and the probe pulse is greater than the situation that pump and
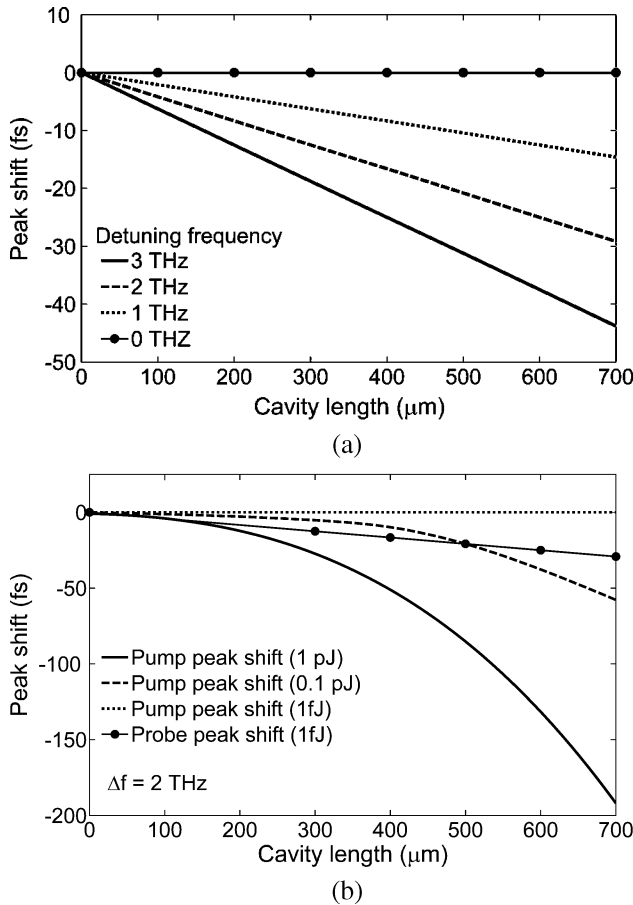
(a)

(b)

Fig. 13. (a) Detuning frequency effects on output probe peak shift and (b) input pump pulse power effects on output pump pulse peak shift versus SOA length.
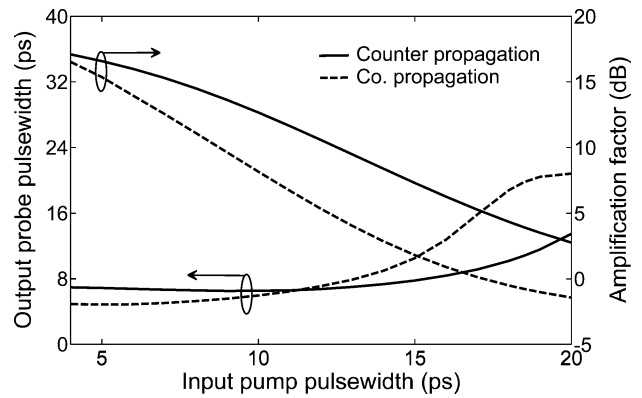

Fig. 14. Comparison between copulse propagation and counterpulse propagation when both pulses are injected simultaneously. The frequency detuning between the two pulses is −1.5 THz. The input probe pulsewidth is 14 ps.
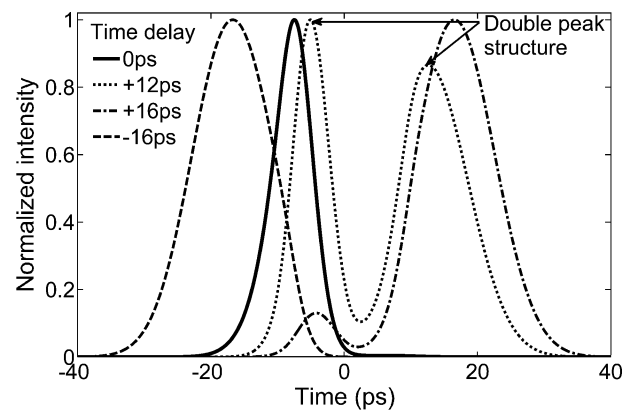

Fig. 15. Normalized output probe pulse shapes at different time delays. The frequency detuning between the two pulses is −1.5 THz.

probe are injected from the opposite facets. So in this case, although better pulse compression can be achieved using the co-propagation scheme, the probe can be amplified more in the counterpropagation scheme due to lower gain saturation effects. As the input pump pulsewidth increases, the overlap between the gain saturated region and the probe pulse decreases, and consequently, we have lower pulse compression effect for both schemes. But, as the pump pulsewidth increases better pulse compression and amplification can be achieved using the counterpropagation scheme compared to the copropagation scheme. It is because in this scheme, trailing edge of probe pulse, encounters the gain saturation region from the beginning of its propagation. So, this effect can efficiently compress this part of probe pulse, but in copropagation scheme the gain saturation only affects the probe pulse from the end of its propagation in SOA waveguide. Besides, better probe amplification factor can be achieved in counterpropagation scheme. This arises because the leading edge of probe pulse can propagate in SOA waveguide without sensing the pump pulse. On the other hand in copropagation scheme entire probe pulse shape is affected by the pump pulse since they propagated together.

The output probe pulse shapes with a 4 ps counterpropagating pump with different time delays are shown in Fig. 15. A negative or positive time delay means that the probe pulse is injected to the SOA before and after the pump pulse, respectively. In negative time delay, when the probe pulse is injected completely

before the pump pulse, the probe pulse is not distorted and achieves maximum gain. An overlap between the probe pulse and pump pulses in the SOA waveguide results in probe pulse distortion. This is because, the trailing edge of the probe pulse experiences less gain rather than its leading edge, which leads to the compression of the probe pulse. When this overlap increases, the probe pulse distortion increases and larger compression occurs. This phenomenon causes a sharper trailing edge as shown in Fig. 15. For a positive time delay, when the probe signal is injected after the pump pulse, a double peak structure is observed, which is due to the comparable gain experienced by two parts of the double peak pulse. The peak that has experienced larger gain (left peak) has shorter width than the right peak which has experienced less gain. As the time delay increases, pump pulse decreases the gain more and so the leading edge of the probe pulse that made the left peak experience less gain and damp rapidly. Finally, the output probe pulsewidth will return that of the input value provided that the normalized peak power of the leading part is less than 0.5 in comparison with the trailing part.

Fig. 16 shows the output pulsewidth of the probe pulse as a function of the time delay for different pump pulse energies. Both pulse compression and broadening for probe pulse is obtained. These effects are achieved just by changing the time delay between pump and probe pulse injection. The sharp changes in output probe pulsewidth are due to the double peak
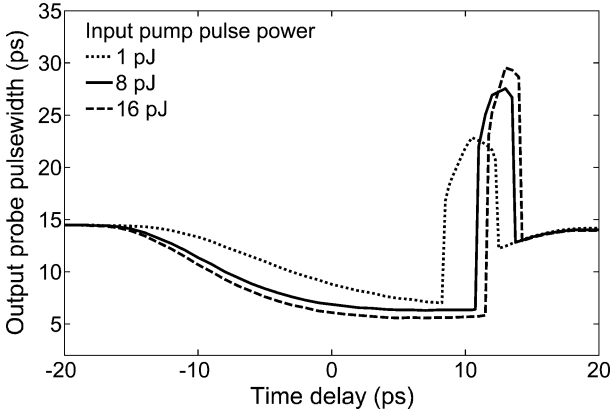
Fig. 16. Output probe pulsewidth as a function of time delay between the counterpropagating probe and pump pulses for different input pump energies.
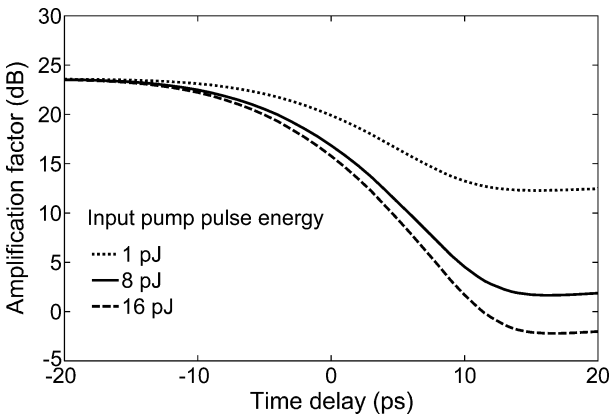

Fig. 17. Amplification factor of the probe pulse versus the time delay between the probe and the pump pulses for different input pump pulse energies.

structure described before. A compression factor as large as 2.2 can be achieved for input pump pulse of 8 pJ with a time delay of 6 ps.

In Fig. 17, the amplification factor for the probe pulse is illustrated. It can be seen that the amplification factor and pulse compression are sensitive to input pump pulse energy. This is due to enhanced carrier depletion caused by higher pump pulse energy, which in turn leads to an enhanced gain modulation experienced by the probe.

This model can be easily applied in subpicosecond regime to investigate the effects of pump pulse on probe pulse shape and spectrum. The counterpropagation scheme has unique feature compared with copropagation scheme where the amplified pulses can be analyzed without using any filtering techniques. In subpicosecond copropagation scheme, the output pulses spectrums are mixed so that probe pulse shape can be hardly distinguishable.

The pulse compression effect is studied for several linearly chirped pulses in subpicosecond regime. In the case of linearly chirped Gaussian pulses, the incident complex amplitude can be written as

$$A^{\pm}(0,t) = (E_{\mathrm{in}}/t_0\sqrt{\pi})^{1/2} \times \exp\left(-(1+iC)/2 \times (t/t_0)^2\right) \tag{19}$$

where E_{in} is the input pulse energy, t_0 is related to input pulse FWHM by $T_{\mathrm{FWHM}} \approx 1.665 t_0$, and C is the chirp parameter.

In subpicosecond regime, for the chirped pulses, the pulse spectrum width becomes comparable to gain spectrum width of the SOA. In the absence of pump pulse, and for the same probe pulsewidth, since the absolute value of the chirp parameter increases, the pulse spectrum becomes wider. So the mutual interaction of the pulse and gain spectrum leads to less broadening effects and consequently lower amplification factor. In this regime, the counterpropagating pump pulse can be used to compress the probe pulse effectively. As the intense pump pulse propagates, the gain behavior of SOA changes so that the pulse compression occurs due to the gain saturation mechanism. The effect of counterpropagating pump pulse on probe pulsewidth for different chirp parameters is shown in Fig. 18. The input probe pulsewidth is 500 fs and its energy is 1 pJ. The pump pulse is unchirped Gaussian and its energy is $E_{\mathrm{sat}}/2$. Based on the results, for -5 and -3 linear chirps, CFP as large as 32% and 15% can be achieved, respectively. These values falls to 5% and -32% in the absence of pump pulse where the positive and negative CFP correspond to the output probe pulse compression and broadening, respectively. It should be noted that the chirp imposed by the SOA on the probe pulse in this case (1 pJ, 500 fs) is negative. Thus, for the probe pulses with negative input chirp, the effect of pulse compression is increased compared with the positive chirp values. Besides, the output probe time-bandwidth (TB) product is always improved compared with its input pulse TB product value as shown in Fig. 19. The input probe TB product for the chirp parameters of ± 5 and ± 3 are 2.24 and 1.4, respectively. With increasing the input pump pulsewidth to 4 ps, these values decrease to 0.58 and 0.63 for corresponding positive C, and similarly to 0.7 and 0.79 for corresponding negative C, respectively. As seen from the Fig. 19, for negatively chirped probe pulses, the pump pulse can significantly compress the probe spectrum width, but for positively chirped pulses the effect of compression in both time and frequency domain is weaker. Fig. 20 shows the amplification factor of the probe pulse corresponding to Fig. 18. The amplification factor of the probe pulse decreases inversely with the pump pulsewidth. This is because of the bigger saturation effects made by the pump pulse. It is shown in Figs. 18–20, we observe that for a given input pump pulsewidth, we have amplified compressed output probe pulse with enhanced TB product.

Based on the results in counterpropagation scheme, spectral changes of probe pulse due to the pump pulse are of great importance.

As shown in Fig. 11, for relatively low-power subpicosecond pulse, the fast process nonlinearities impose mainly a positive chirp on the propagated pulse. Thus, output probe spectrum is shifted to blue side. To investigate the pump pulse effect on probe pulse, the pump energy and pulsewidth are selected so that a meaningful change in probe spectrum occurs. Fig. 21 shows the effects of different counterpropagating pump energies on the probe spectrum. Both pump and probe input pulses are unchirped Gaussian. The unsaturated gain is 30 dB. The 500 fs probe pulse energy is 1 fJ and the pump pulsewidth is 5 ps. As the input pump energy approaches the saturation energy of SOA, its effects on the probe pulse spectrum becomes more ap-
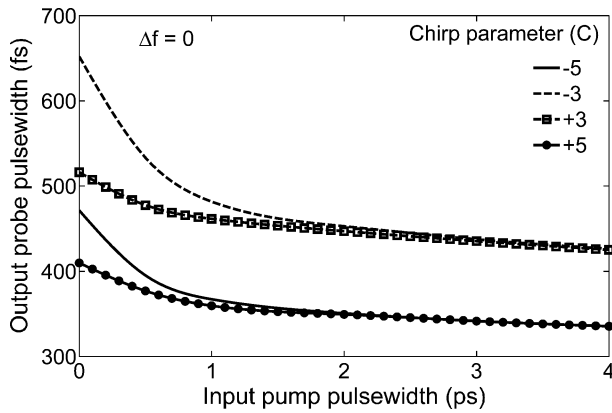
Fig. 18. Output probe pulsewidth versus pulsewidth of counterpropagating input pump for different initial chirp parameters. Input probe pulsewidth is 500 fs.
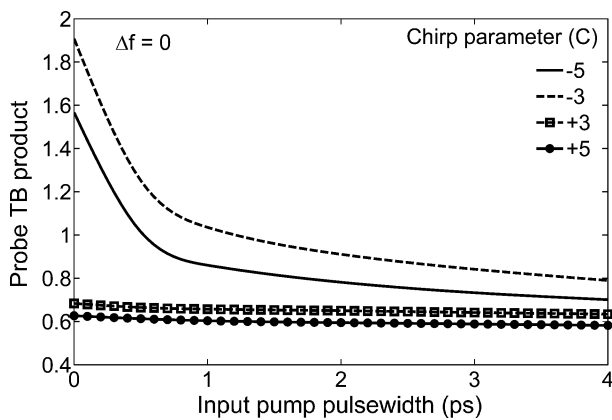

Fig. 21. Normalized output probe spectrum for different energies of counterpropagating pump pulse. The input pump and probe pulsewidth are 5 ps and 500 fs, respectively.

Fig. 19. Output probe TB product versus pulsewidth of counterpropagating input pump.

Fig. 22. Normalized output probe spectrum for different pulsewidths of counterpropagating pump pulse, while the pump energy is $E_{\mathrm{sat}}/2$.
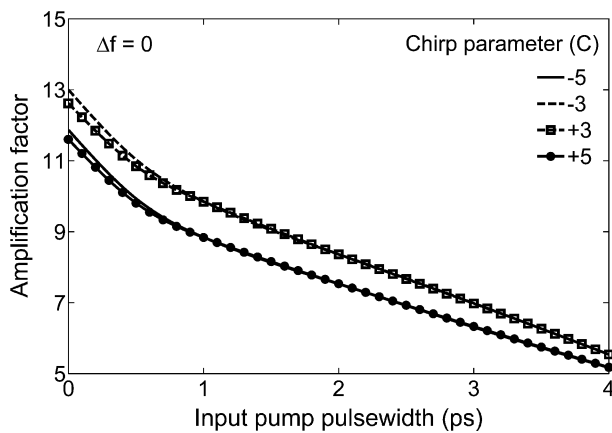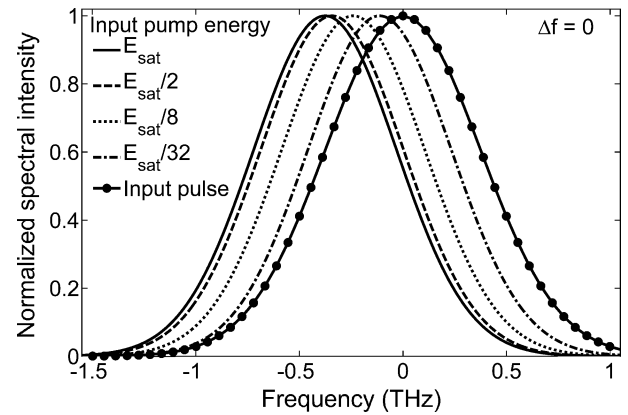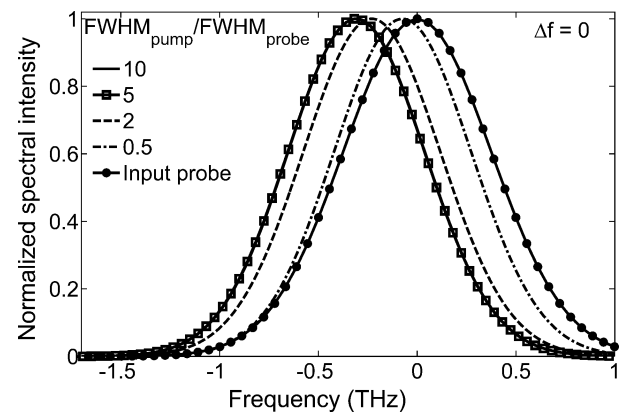

Fig. 20. Output probe amplification factor versus pulsewidth of counterpropagating input pump.

parent. In this regime, the SOA gain is modulated by the pump pulse, resulting in imposition of negative chirp on the amplified probe. This effect shifts the output probe spectrum to the red side as shown in Fig. 21. The output probe spectral peak position can also be changed by the pump pulsewidth. Fig. 22 shows that as the pump pulsewidth increases, the effect of saturation mechanism on probe pulse becomes greater. The maximum probe spectral peak shift (PSPS) occurs for the pump

pulsewidths around 5 ps. For wider pump pulses, the probe amplification factor decreases, while there is no considerable change in output probe spectral peak position.

Fig. 23 shows the PSPS due to a counterpropagating pump pulse versus the input probe pulsewidth for different detuning frequencies. In this case, for each input probe pulsewidth, the corresponding input pump pulsewidth is taken ten times larger, and pump energy is equal to $E_{\mathrm{sat}}/2$. Based on the results, as the input probe pulsewidth decreases, the effects of pump pulse on probe spectrum become greater. This is because in subpicosecond regime as the probe pulsewidth is shorter than SOA propagation time, the time in which the entire pulse spectrum interacts with SOA medium increases and the propagated pulse spectrum becomes more affected by SOA nonlinearities compared with wider pulses. It should be noted that in the subpicosecond regime, the results are reliable when all fast process nonlinear effects are included in the model. In addition, in this regime, since the input pulse and SOA gain medium spectrum width become comparable, the effect of gain dispersion nonlinearity has a significant effect on the probe pulse. Therefore, relatively high-power pump pulse which modulates the SOA behavior, significantly changes the probe spectrum. Besides, the effect of detuning frequency on PSPS is also illustrated in Fig. 23. Results show that PSPS as large as 0.7 THz can be
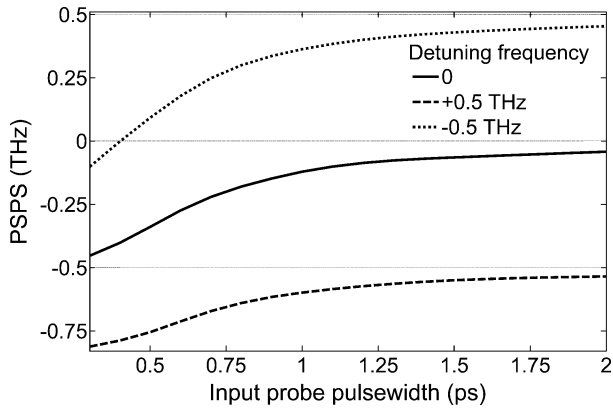
Fig. 23. PSPS versus input probe pulsewidth in different detuning frequencies. The counterpropagating pump pulsewidth is ten times larger than the probe input pulsewidth.
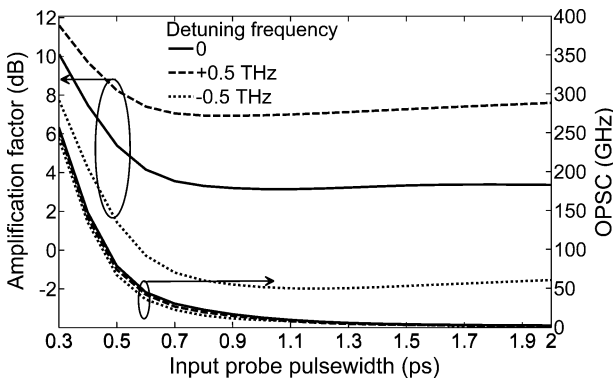

Fig. 24. Output probe spectrum compression and amplification factor versus input probe pulsewidth. The input parameters are the same as Fig. 23.

achieved for 300 fs probe pulse and -0.5 THz detuning frequency. This value decreases to 0.45 THz and 0.3 THz for 0 and 0.5 THz detuning frequencies, respectively for the same probe pulsewidth.

Fig. 24 shows the output probe spectral compression (OPSC), left axis, and its amplification factor, right axis, versus input probe pulsewidth for different detuning frequencies. OPSC is defined as the difference between input and output probe spectral width. Although the effect of pump pulse on probe spectrum in negative detuning frequencies is weaker compared to positive detuning frequencies, better amplification factor for the probe pulse can be achieved in this case as shown in Fig. 24. Besides probe amplification, probe spectrum width is also noticeably compressed in the subpicosecond regime for different detuning frequencies.

IV. CONCLUSION

An improved and computationally efficient finite-difference time-dependent BPM was developed in this paper. The technique was applied to solve MNLSEs, including a large range of nonlinear effects, to copropagating and counterpropagating pulses in an SOA. We numerically analyzed nondegenerate FWM in short optical pulses and the effects of collision between counterpropagating pulses. Our results showed excellent agreement with copropagation and counterpropagation results reported elsewhere. The effects of intense pump pulse on probe

pulse in copropagation and counterpropagation schemes were compared. The effects of counterpropagating pump pulse on subpicosecond probe pulses were also studied. It was shown that in this regime, the pump pulse can effectively compress the probe pulsewidth while the pump pulse can significantly decrease the amplified probe TB product. Furthermore, based on our results, output probe spectrum peak was shifted due to the effects of counterpropagating pump pulses. The value of this shift was controlled by the pump power and pulsewidth. In addition, the probe pulse was amplified and its spectral width was compressed simultaneously.

REFERENCES

[1] M. J. Connelly, *Semiconductor Optical Amplifiers.* Boston, MA: Kluwer, 2002.

[2] R. Gutiérrez-Castrejón, L. Schares, L. Occhi, and G. Guekos, "Modeling and measurement of longitudinal gain dynamics in saturated semiconductor optical amplifiers of different length," *IEEE J. Quantum Electron.*, vol. 36, no. 12, pp. 1476–1484, Dec. 2000.

[3] L. Occhi, L. Schares, and G. Guekos, "Phase modeling based on the α-factor in bulk semiconductor optical amplifiers," *IEEE J. Sel. Topics Quantum. Electron.*, vol. 9, no. 3, pp. 788–797, May/Jun. 2003.

[4] H. J. S. Dorren, G. D. Khoe, and D. Lenstra, "All-optical switching of an ultrashort pulse using a semiconductor optical amplifier in a Sagnac-interferometric arrangement," *Opt. Commun.*, vol. 205, no. 4–6, pp. 247–252, 2002.

[5] H. J. S. Dorren, D. Lenstra, L. Yong, M. T. Hill, and G. D. Khoe, "Non-linear polarization rotation in semiconductor optical amplifiers: Theory and application to all-optical flip-flop memories," *IEEE J. Quantum Electron.*, vol. 39, no. 1, pp. 141–148, Jan. 2003.

[6] K. E. Stubkjaer, "Semiconductor optical amplifier-based all-optical gates for high-speed optical processing," *IEEE J. Sel. Topics Quantum. Electron.*, vol. 6, no. 6, pp. 1428–1435, Nov./Dec. 2000.

[7] C. G. Lee, Y. J. Kim, and C.-S. Park, "Optical pulse shaping by cross-phase modulation in a harmonic mode-locked semiconductor fiber ring laser under large cavity detuning," *J. Lightw. Technol.*, vol. 24, no. 3, pp. 1237–1246, 2006.

[8] D. Nesset, T. Kelly, and D. Marcenac, "All-optical wavelength conversion using SOA nonlinearities," *IEEE Commun. Mag.*, vol. 36, no. 12, pp. 56–61, Dec. 1998.

[9] A. Hamié, A. Sharaiha, M. Guegan, and J. L. Bihan, "All-optical inverted and noninverted wavelength conversion using two-cascaded semiconductor optical amplifiers," *IEEE Photon. Technol. Lett.*, vol. 17, no. 6, pp. 1229–1231, Jun. 2005.

[10] M. Amaya, A. Sharaiha, and F. Ginovart, "Comparison between co- and counter-propagative optical injection near the transparency wavelength on SOA static and dynamic performances," *Opt. Commun.*, vol. 246, no. 1–3, pp. 67–71, 2005.

[11] A. Sharaiha and A. Hamie, "Comprehensive analysis of two cascaded semiconductor optical amplifiers for all-optical switching operation," *J. Lightw. Technol.*, vol. 22, no. 3, pp. 850–858, 2004.

[12] S. Bischoff, A. Buxens, H. N. Poulsen, A. T. Clausen, and J. Mørk, "Bidirectional four-wave mixing in semiconductor optical amplifiers: Theory and experiment," *J. Lightw. Technol.*, vol. 17, no. 9, pp. 1617–1625, 1999.

[13] G. P. Agrawal and N. A. Olsson, "Self-phase modulation and spectral broadening of optical pulses in semiconductor laser amplifiers," *IEEE J. Quantum Electron.*, vol. 25, no. 11, pp. 2297–2306, Nov. 1989.

[14] L. Schares, C. Schubert, C. Schmidt, H. G. Weber, L. Occhi, and G. Guekos, "Phase dynamics of semiconductor optical amplifiers at 10–40 GHz," *IEEE J. Quantum Electron.*, vol. 39, no. 11, pp. 1394–1408, Nov. 2003.

[15] A. Mecozzi and J. Mørk, "Saturation effects in nondegenerate four-wave mixing between short optical pulses in semiconductor laser amplifiers," *IEEE J. Sel. Topics Quantum. Electron.*, vol. 3, no. 5, pp. 1190–1207, Oct. 1997.

[16] P. Borri, S. Scaffetti, J. Mørk, W. Langbein, J. M. Hvam, A. Mecozzi, and F. Martelli, "Measurement and calculation of the critical pulsewidth for gain saturation in semiconductor optical amplifiers," *Opt. Commun.*, vol. 164, no. 1–3, pp. 51–55, 1999.

[17] R. S. Grant and W. Sibbet, "Observations of ultrafast nonlinear refraction in an InGaAsP optical amplifier," *Appl. Phys. Lett.*, vol. 59, no. 11, pp. 1119–1121, 1991.

[18] M. Y. Hong, Y. H. Chang, A. Dienes, J. P. Heritage, and P. J. Delfyett, "Subpicosecond pulse amplification in semiconductor laser amplifiers: Theory and experiment," *IEEE J. Quantum Electron.*, vol. 30, no. 4, pp. 1122–1131, Apr. 1994.

[19] J. M. Tang and K. A. Shore, "Strong picosecond optical pulse propagation in semiconductor optical amplifiers at transparency," *IEEE J. Quantum Electron.*, vol. 34, no. 7, pp. 1263–1269, Jul. 1998.

[20] K. Obermann, S. Kindt, D. Breuer, and K. Petermann, "Performance analysis of wavelength converters based on cross-gain modulation in semiconductor-optical amplifiers," *J. Lightw. Technol.*, vol. 16, no. 1, pp. 78–85, 1998.

[21] Y. Kim, H. Lee, S. Kim, J. Ko, and J. Jeong, "Analysis of frequency chirping and extinction ratio of optical phase conjugate signals by four-wave mixing in SOA's," *IEEE J. Sel. Topics Quantum. Electron.*, vol. 5, no. 3, pp. 873–879, May/Jun. 1999.

[22] A. E. Willner and W. Shieh, "Optimal spectral and power parameters for all-optical wavelength shifting: Single stage, fanout, and cascadability," *J. Lightw. Technol.*, vol. 13, no. 5, pp. 771–781, 1995.

[23] N. K. Das, Y. Yamayoshi, and H. Kawaguchi, "Analysis of basic four-wave mixing characteristics in a semiconductor optical amplifier by the finite-difference beam propagation method," *IEEE J. Quantum Electron.*, vol. 36, no. 10, pp. 1184–1192, Oct. 2000.

[24] T. Durhuus, B. Mikkelsen, and K. E. Stubkjaer, "Detailed dynamic model for semiconductor optical amplifiers and their crosstalk and intermodulation distortion," *J. Lightw. Technol.*, vol. 10, no. 8, pp. 1056–1065, 1992.

[25] G. Toptchiyski, S. Kindt, K. Petermann, E. Hilliger, S. Diez, and H. G. Weber, "Time-domain modeling of semiconductor optical amplifiers for OTDM applications," *J. Lightw. Technol.*, vol. 17, no. 12, pp. 2577–2583, 1999.

[26] J. W. D. Chi, C. Lu, and M. K. Rao, "Time-domain large-signal investigation on nonlinear interactions between an optical pulse and semiconductor waveguides," *IEEE J. Quantum Electron.*, vol. 37, no. 10, pp. 1329–1336, Oct. 2001.

[27] R. Scarmozzino, A. Gopinath, R. Pregla, and S. Helfert, "Numerical techniques for modeling guided-wave photonic devices," *IEEE J. Sel. Topics Quantum. Electron.*, vol. 6, no. 1, pp. 150–162, Jan./Feb. 2000.

[28] J. Shibayama, A. Yamahira, T. Mugita, J. Yamauchi, and H. Nakano, "A finite-difference time-domain beam-propagation method for TE- and TM-wave analyses," *J. Lightw. Technol.*, vol. 21, no. 7, pp. 1709–1715, 2003.

[29] C. Ma and E. Van Keuren, "A three-dimensional wide-angle BPM for optical waveguide structures," *Opt. Exp.*, vol. 15, no. 2, pp. 402–407, 2007.

[30] M. Y. Hong, Y. H. Chang, A. Dienes, J. P. Heritage, P. J. Delfyett, S. Dijaili, and F. G. Patterson, "Femtosecond self- and cross-phase modulation in semiconductor laser amplifiers," *IEEE J. Sel. Topics Quantum. Electron.*, vol. 2, no. 3, pp. 523–539, Sep. 1996.

[31] L. M. Zhang, S. F. Yu, M. C. Nowell, D. D. Marcenac, J. E. Carroll, and R. G. S. Plumb, "Dynamic analysis of radiation and side-mode suppression in a second-order DFB laser using time-domain large-signal traveling wave model," *IEEE J. Quantum Electron.*, vol. 30, no. 6, pp. 1389–1395, Jun. 1994.

[32] H. Adachihara, R. A. Indik, and J. V. Moloney, "Semiconductor laser array dynamics: Numerical simulations on multistripe index-guided lasers," *J. Opt. Soc. Am. B*, vol. 10, no. 3, p. 496, 1993.

[33] W. H. Press, S. A. Teukolsky, B. P. Flannery, and W. T. Vetterling, *Numerical Recipes in Fortran*, 2nd ed. Cambridge, U.K.: Cambridge Univ. Press, 1992.

[34] G. P. Agrawal, *Nonlinear Fiber Optics*, 3rd ed. New York: Academic Press, 2001.

[35] C. M. de Sterke, K. R. Jackson, and B. D. Robert, "Nonlinear coupled-mode equations on a finite interval: A numerical procedure," *J. Opt. Soc. Am. B*, vol. 8, no. 2, p. 403, 1991.

[36] C. M. Fernandez, P. Morel, and J. W. D. Chi, "Temporal and spectral properties of contra-propagating picosecond optical pulses in SOA," *Opt. Commun.*, vol. 259, no. 2, pp. 465–469, 2006.

[37] J. M. Tang and K. A. Shore, "Active picosecond optical pulse compression in semiconductor optical amplifiers," *IEEE J. Quantum Electron.*, vol. 35, no. 1, pp. 93–100, Jan. 1999.

Mohammad Razaghi (S'08) was born in Chandigarh, India, in 1979. He received the B.S. degree from Razi University, Kermanshah, Iran, in 2001, and the M.S. degree from Tarbiat Modares University, Tehran, Iran, in 2003, both in electrical engineering, where currently he is working toward the Ph.D. degree in the same field.

He spent a sabbatical period, during 2007–2008, with Optical Communication Research Group, University of Limerick, Ireland. His current research interests include applications of nonlinear optics in semiconductor optoelectronic devices, optical pulse shaping, and optical fiber communications.

Vahid Ahmadi (M'86) received the Ph.D. degree in electronic engineering from the Kyoto University, Japan, in 1994.

He is a Professor in electronic engineering at Tarbiat Modares University (TMU), Tehran, Iran. From 1994 to 2006, he was the Head of the Semiconductor Department of Laser Research Centre, Tehran. He has been the Head of the Electrical Engineering Department of TMU, during 2006–2008. He was the technical and scientific Chair of 13th Iranian Conference on Optics and Photonics, 2007, and the general Chair of the 16th Iranian Conference on Electrical Engineering (ICEE2008), 2008. His current research interests include quantum photonics devices, optical modulator and amplifiers, optical microresonator active and passive devices, optical switches, slow light, and photonic crystals.

Dr. Ahmadi is the member of the Founders-Board of Optics and Photonics Society of Iran.

Michael J. Connelly (S'89–M'92) received the Ph.D. degree in electronic engineering from the National University of Ireland, Dublin, in 1992.

He is a Senior Lecturer in electronic engineering and the Director of the Optical Communications Research Group at the University of Limerick, Ireland. The current research interests of the Group include all-optical signal processing using semiconductor optical amplifiers, fiber ring lasers, and optical coherence.